IOP Publishing Superconductor Science and Technology
Supercond. Sci. Technol. **29** (2016) 034001 (11pp) doi:10.1088/0953-2048/29/3/034001

A superconducting homopolar motor and generator—new approaches

Rene Fuger, Arkadiy Matsekh, John Kells, D B T Sercombe and Ante Guina

Guina Energy Technologies Pty Ltd, 31 Harrington Street, Arundel 4214 QLD, Australia

E-mail: rene@guinaenergy.com

Received 24 August 2015, revised 2 November 2015
Accepted for publication 10 November 2015
Published 22 January 2016

Abstract

Homopolar machines were the first continuously running electromechanical converters ever demonstrated but engineering challenges and the rapid development of AC technology prevented wider commercialisation. Recent developments in superconducting, cryogenic and sliding contact technology together with new areas of application have led to a renewed interest in homopolar machines. Some of the advantages of these machines are ripple free constant torque, pure DC operation, high power-to-weight ratio and that rotating magnets or coils are not required. In this paper we present our unique approach to high power and high torque homopolar electromagnetic turbines using specially designed high field superconducting magnets and liquid metal current collectors. The unique arrangement of the superconducting coils delivers a high static drive field as well as effective shielding for the field critical sliding contacts. The novel use of additional shielding coils reduces weight and stray field of the system. Liquid metal current collectors deliver a low resistance, stable and low maintenance sliding contact by using a thin liquid metal layer that fills a circular channel formed by the moving edge of a rotor and surrounded by a conforming stationary channel of the stator. Both technologies are critical to constructing high performance machines. Homopolar machines are pure DC devices that utilise only DC electric and magnetic fields and have no AC losses in the coils or the supporting structure. Guina Energy Technologies has developed, built and tested different motor and generator concepts over the last few years and has combined its experience to develop a new generation of homopolar electromagnetic turbines. This paper summarises the development process, general design parameters and first test results of our high temperature superconducting test motor.

Keywords: liquid metal current collectors, unipolar machine, DC motor

(Some figures may appear in colour only in the online journal)

1. Introduction

History shows that homopolar machines are well known for their simplicity and high efficiency but also for their high electric currents and magnetic fields. Both high currents and magnetic fields are difficult to handle and historically have been viewed as problematic with this type of machine. Although the hompolar machines have not been widely commercialised, considerable research has been undertaken related to high current sliding contacts and magnet technology for these types of machines. This research resulted in several prototype machines which were in operation for an extended period of time with excellent performance [1, 2]. The importance of these two technologies for the operation of the machine is evident given the correlation between advances in brush and magnet technology and subsequent development of homopolar machines.

Different brush technologies were developed and tested extensively at the beginning of the 20th century due to the increased need for high power generators [3]. Soon the advantage of liquids as the contact material between the stationary and moving components was demonstrated and early prototypes with liquid metal current collectors (LMCC) were built [4]. This technology reached its peak development in the 1960s leading to high power homopolar electric generators that were used as current sources [5]. Recently, metal fibre

brushes [6] have been viewed as an alternative to LMCC due to their simpler implementation but metal fibre brushes cannot achieve the high surface speeds and current densities of LMCC. Both LMCC and metal fibre brushes cannot work in high magnetic fields due to the Lorentz forces acting on them.

Early homopolar machines used large water cooled electromagnets and a lot of iron to guide the magnetic field, making them very heavy devices [7]. The development of superconducting magnets in the 1960s, that could achieve much higher magnetic fields using less power and having a smaller size, initiated new interest in homopolar machines. Whereas the early machines were focused on generators for electricity production, superconducting technology enabled the development of homopolar machines for applications that are more weight and size critical, such as ship propulsion [8, 9]. However, with increasing magnetic field the stray field and brush shielding became more of a problem. Another difficulty was the cryogenic cooling of the magnets and the stability of operation in rough environments. Recent improvements in cryogenic technologies and the development of high-temperature superconductor wire make the cryogenic system more efficient and simpler.

In this paper we present our unique approach to high power and high torque superconducting homopolar electromagnetic turbines which overcome the problems mentioned above. First, the operating principle of homopolar motors and the basic parameters will be discussed. Then we present our uniquely designed coil arrangement which provides both the high drive field and shielding for the field critical current collector area. A short section about our LMCC explains the principle of operation and the basic parameters of this system. Next we introduce our 200 kW test motor design and present our first test results. Finally, we provide an outlook on possible applications and the advantages of our machines.

2. Operating principle

The homopolar motor is a pure DC machine without commutator or varying magnetic fields. The main components of the machine are the magnet, the moving part of the current loop (rotor), the sliding contacts and the return path of the current loop (stator). The magnetic field producing coils or magnets are neither part of the rotor nor the stator of the machine, hence there is no torque reaction on them. It is important that the magnetic field is rotationally symmetric to avoid eddy currents or drag forces influencing the machine performance. The stator and rotor are different parts of the current carrying loop separated by two sliding contacts which allow them to move relative to one other. The loop is penetrated by the magnetic field, creating reaction forces on the different conductor parts resulting in a zero net force. There are two main types of homopolar motors, the disc type and drum type, which differ in the way the field is oriented relative to the rotating axis.

2.1. Disc type

The principle of a disc type homopolar motor is shown in figure 1. The motor consists of a conducting disc with a shaft (rotor), a brush on the disc outer circumference and one on the shaft (sliding contacts), a return current path (stator) and the magnetic field. The field producing coils or magnets are not shown in the figure and the field is assumed to be rotationally symmetric and orientated parallel to the shaft. The electric field equation for the current loop is given by:

$$\oint_L \boldsymbol{E}\cdot\boldsymbol{dl} = \int_{r_{in}}^{r_{out}} E_r \mathrm{d}r + \int_{r_{out}}^{r_{in}} \boldsymbol{E}\cdot\boldsymbol{dl} = 0, \tag{1}$$

where the first part of the equation describes the voltage potential generated by the rotating disc and the second part the source voltage. E_r is the radial electric field evaluated by the Faraday's law for the current path between inner and outer disc radius. Without taking the brush and conductor losses into account the equation can be rewritten to:

$$\int_{r_{out}}^{r_{in}} \boldsymbol{E}\cdot\boldsymbol{dl} = v_r = \int_{r_{in}}^{r_{out}} \left(\frac{i_r}{2\pi r\sigma d} - \omega r B_0\right) \times \mathrm{d}r = \frac{i_r}{2\pi\sigma d}\ln\frac{r_{out}}{r_{in}} - \frac{\omega B_0}{2}({r_{out}}^2 - {r_{in}}^2), \tag{2}$$

where σ is the conductivity, ω the angular velocity, r_{in} and r_{out} are respectively the inner and outer radius of the rotor, d the disc thickness, i_r the radial rotor current and B_0 the magnetic field. The open circuit voltage (v_{oc}) is determined by the second part of the equation when the rotor current is set to zero:

$$v_{oc} = -\frac{\omega B_0}{2}({r_{out}}^2 - {r_{in}}^2) \tag{3}$$

and the short circuit current (i_{sc}) can be calculated by:

$$i_{sc} = \frac{-\frac{\omega B_0}{2}({r_{out}}^2 - {r_{in}}^2)}{\ln\frac{r_{out}}{r_{in}}} 2\pi\sigma d = \frac{v_{oc}}{\ln\frac{r_{out}}{r_{in}}} 2\pi\sigma d. \tag{4}$$

Solving these equations for different nominal parameters shows that homopolar machines typically operate at low voltages and high currents. The voltage is determined by the magnetic field strength, the angular speed and the inner and outer radius (working length). Higher voltages would be preferable in order to reduce electrical losses in the brushes and enable a smaller conductor cross-section. A stronger magnetic field, such as that provided by superconducting magnets, leads to higher voltage and therefore to smaller and lighter machines.

The electromagnetic torque can be calculated by the Lorentz force acting on the rotor

$$\boldsymbol{F} = q(\boldsymbol{E} + \boldsymbol{v}\times\boldsymbol{B}) \tag{5}$$

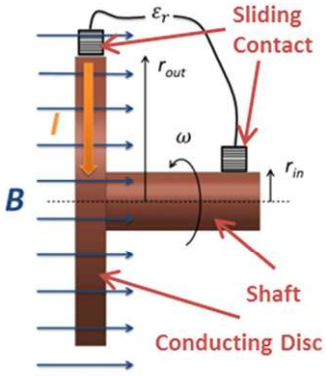

Figure 1. A simple sketch of a disc type homopolar machine and indicates the basic machine parameters.

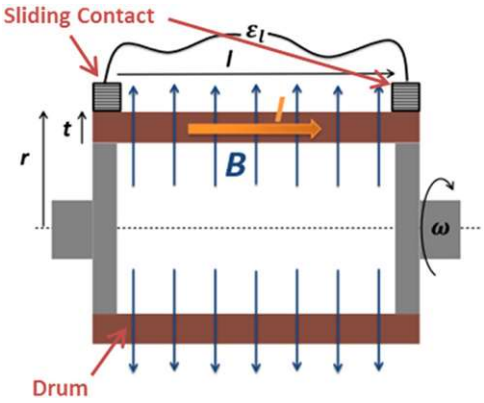

Figure 2. A sketch of a drum type homopolar machine and indicates the basic machine parameters.

$$\boldsymbol{\tau} = \boldsymbol{r} \times \boldsymbol{F} = \int_{\phi=0}^{2\pi}\int_{z=0}^{d}\int_{r=r_{\text{in}}}^{r_{\text{out}}} r\, i_{\text{r}} \times (J \times B)\, r\, \mathrm{d}r\, \mathrm{d}\phi\, \mathrm{d}z$$
$$= -i_{\text{r}} B_0 i_z \int_{r_{\text{in}}}^{r_{\text{out}}} r\, \mathrm{d}r = -i_{\text{r}} B_0 ({r_{\text{out}}}^2 - {r_{\text{in}}}^2) i_z. \quad (6)$$

The equation can be simplified by assuming a uniform magnetic field that is parallel to the rotor axis and a current (I) flowing only in radial direction ($i_z = 0$) through the disc.

$$\tau = \int_{r_{\text{in}}}^{r_{\text{out}}} I\, B_{(r)}\, r\, \mathrm{d}r \quad (7)$$

$$P = \boldsymbol{\tau} \cdot \boldsymbol{\omega}. \quad (8)$$

Higher magnetic fields result in a more powerful machine or smaller machine size for the same power.

2.2. Drum type

In the drum type homopolar motor (figure 2) the magnetic field is orientated in the radial direction and the current carrying rotor component is parallel to the rotor axis (drum surface). The magnetic field has to be constant along the circumference but can vary along the length of the drum. Now, the radius of the drum is no longer equal to the working length (the part of the rotor upon which the forces act) of the machine. The working length is now determined by the distance between the brushes which is normally determined by the length of the drum. Again, the field producing coils or magnets are not shown in the figure. Similar calculations to the disc type homopolar machine can be performed to determine the voltage and torque of the drum type motor.

$$v_l = \int_0^l \left(\frac{I}{2\pi\left(r - \frac{t}{2}\right)t\sigma} - \omega r B(l) \right) \mathrm{d}l \quad (9)$$

$$\tau_l = \int_0^l I\, B(l)\, r\, \mathrm{d}l, \quad (10)$$

where σ is the conductivity, ω the angular velocity, r the drum radius, l the drum length, t the drum thickness and $B(l)$ the magnetic field along the drum length. An increase in field strength results in higher voltage and torque that increases the machine performance or allows a smaller size for similar power. This type of machine has the advantage that the radius and length can be varied separately, however the average magnetic field typically decreases rapidly with larger working lengths. Our designs concentrate on disc type machines but the principles and technologies can be also applied to drum type machines.

2.3. Design parameters

When designing a homopolar motor the main operating parameters have to be matched to the application. Torque, speed and power are the main parameters that are normally predefined but detailed specifications on size limits, maximum weight, efficiency and operating conditions influence the optimum design. By varying the field strength, maximum current or working length the machine can be optimised to meet the requirements of the application, such as target efficiency, energy density or the operating environment. Compared with other machines the relationship between the motor parameters and power output is simple and given by the equations above. Limits for the different components of the machine are given by the properties of the materials and technologies used. Table 1 summarises some of the limitations and operating parameters considered as practical for our machines.

3. Magnet field design

The magnet design directly influences the machine's weight, size, efficiency and power (as shown previously) but they are not part of the stator or the rotor of the machine. Therefore they are not subject to mechanical motion, reaction torque and field or current variation. The pure DC environment is a big advantage when compared with conventional machines where AC losses are a big issue. Furthermore, superconducting DC magnets are a well developed technology and are manufactured in large quantities for MRI's and other applications. The magnet system required for the homopolar machine is

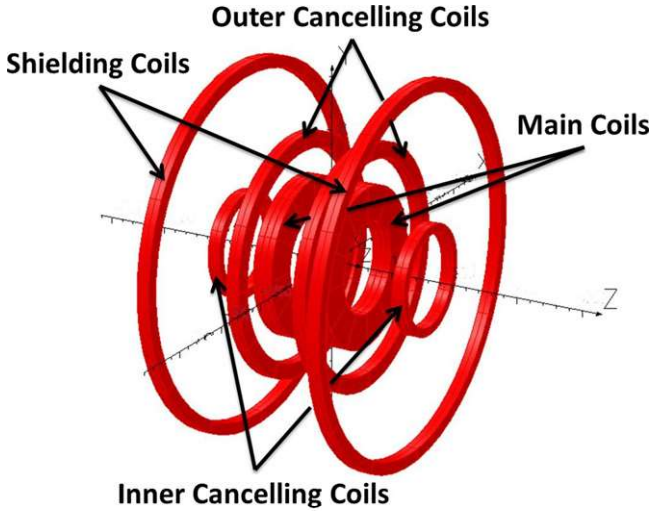

Figure 3. Basic superconducting coil arrangement in Guina disc type homopolar machines.

similar to these magnet systems. Another advantage is the separation of the magnet system from the rotor and stator which allows more flexibility in the design and manufacturing process.

We have developed a coil arrangement that implement new approaches to improve the performance of homopolar machines [10]. Guina Energy Technologies' unique superconducting coil system consists of main, cancelling and shielding coils (figure 3).

This arrangement creates a high drive field and while effectively shielding stray field at the same time. A complex field profile containing both high field areas, up to several Tesla, and regions with fields not exceeding a few hundredths of a Tesla are generated in our machine. The low field regions are required to protect the LMCC from excessive magnetic fields which would create additional losses or prevent their proper operation. Active shielding reduces the amount of heavy iron shielding material and overcomes the problem of material saturation. We have developed different coil arrangements that allow different positions of the low field regions depending on the machine requirements [10]. The concept presented in this manuscript is one of the simpler designs and was also chosen for our prototype motor. The coil arrangement and positioning was analysed using finite element software (COBHAM Vector Fields Opera software) and the field calculations are based on superconducting wire specifications provided by the manufacturer as well as typical manufacturing limitations. Currently different types of superconducting wires are available which can be used to manufacture the coils for the magnets. Our simulations provided us with the physical limits for the various superconducting wires however it is also important to consider the relative costs and availability of these wires. Whereas high temperature superconductors have the advantage of employing simpler cryostats due to higher operating temperatures and high critical fields, the high cost of HTS wires is problematic. The concept presented in this paper is not limited to any specific type of conductor. The maximum field reached in the machine depends on the superconducting material used for the magnets. In this paper the term high field area refers to regions where the magnetic field strengths are above 1 T (reaching up to 12 T) whereas low field areas denote regions that are normally only a few hundreds of milli Tesla or lower.

3.1. Low-field regions

The low-field regions have to be situated close to the driving magnetic field to avoid unnecessarily long current paths between the working area (region with high drive field) and the brushes. Figure 4 shows the field profile and coil arrangement for our disc type magnet system which was used for our test motor. The split pair arrangement consists of the main coils (a) and cancelling coils (b) which are symmetric about the rotor central axis. The main coils generate the drive field for the rotor and they are the coils with the highest magnetic fields. Two sets of cancelling coils, outer cancelling coils close to the disc circumference and inner cancelling coils close to the ends of the shaft generate areas with reduced fields on the outer circumference of the rotor and on both ends of the shaft. These coils are also reducing the stray field of the whole magnet system. Other designs are possible where the low field region situated on the shaft can be positioned just on one side or in the centre of the magnet.

The field profile indicates areas with high magnetic fields in red and low field areas in blue. The contour lines separate areas with 1/10 (red), 1/25 (orange), 1/50 (green) and 1/100 (blue) of the maximum field. The LMCC are situated in the very low field region, area outside the green contour lines, as indicated in the figure. Similar low field regions can be achieved in drum type machines by separating the main coils into four coils as shown in figure 5. Specially designed cryostats, which allow access to the low field region in the middle, had to be constructed to enable the brush system to be positioned in the low field region. There are no additional cancelling coils required but the arrangement and field produced by the individual coils had to be given careful consideration. Other variations of coil arrangements are also possible which allow access to the low field regions from the top or bottom of the magnet [10].

3.2. Active shielding

To reduce the stray field further, Guina Energy Technologies has developed an active shielding system featuring two, four or five shielding coils, similar to those used in MRI magnets [10]. Depending on the application requirements, government regulations, and safety issues, the 200 Gauss line can be brought right onto the surface of the machine, even for high field magnets of several Tesla. Figure 6 shows the 200 and 5 Gauss boundary lines for an unshielded system and a 2 and 4 shielding coil arrangement. The shielded magnet systems require about 1/3 more superconducting wire and increase the diameter of the machine envelope when compared with the completely unshielded design. However, considering the large amount of iron that would be required to reduce the stray field to acceptable values, these actively shielded

Table 1. Critical parameters for different machine components considering current technologies.

	Current technology limitations	Guina maximum design parameters
Brush current density	~40 A cm^{-2} Silver graphite solid brushes	
	~150 A cm^{-2} Metal fibre brushes	Liquid metal current collectors
	~500 A cm^{-2} Liquid metal current collectors	100–500 A cm^{-2}
	>500 A cm^{-2} Liquid metal spray systems	
Magnetic field	<0.6 T (permanent magnets)	Superconducting magnet
	<2 T (electromagnets)	5–12 T
	<21 T (superconductor)	
Radius	Mechanical limits applies for weight and stress	0.4–3 m
Surface speed	~15 m s^{-1} Silver graphite solid brushes	
	~60 m s^{-1} Metal fibre brushes	Liquid metal current collectors
	~200 m s^{-1} Liquid metal current collectors	30–120 m s^{-1}
	>200 m s^{-1} Liquid metal spray systems	

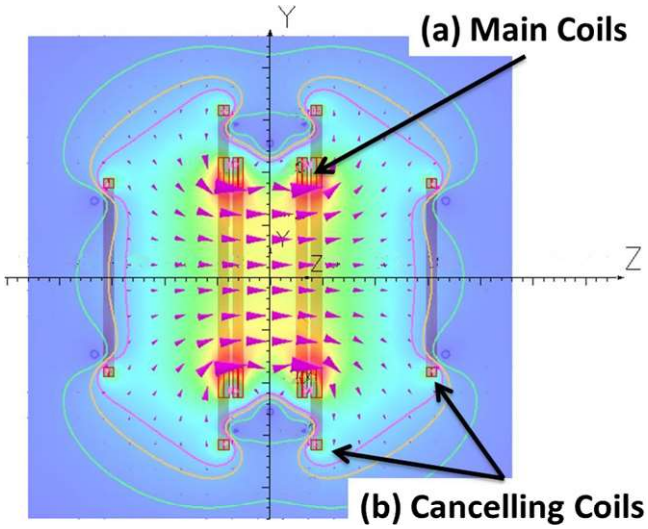

Figure 4. Magnet field profile for disc type homopolar machine with cancelling coils. Areas with high magnetic fields (maximum 2.4 T) are shown in red and areas with low magnetic field are shown in blue. The contour lines separate areas with 1/10 (red), 1/25 (orange), 1/50 (green) and 1/100 (blue) of the maximum field.

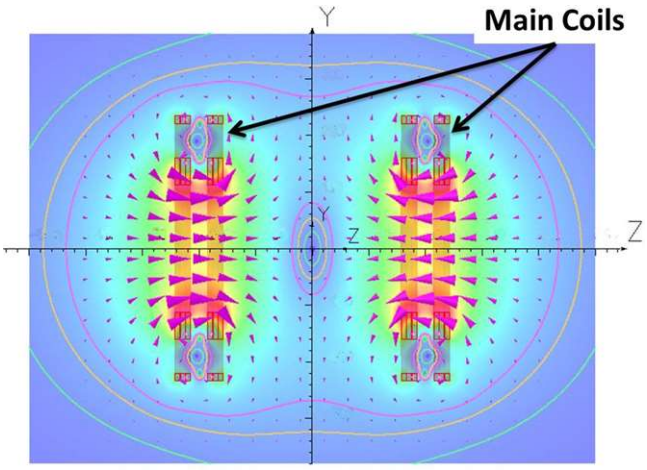

Figure 5. Magnetic field profile for a drum type homopolar machine with low-field regions. Areas with high magnetic fields (maximum 3 T) are shown in red and areas with low magnetic field are shown in blue. The arrows indicating the magnetic field direction. The contour lines separate areas with 1/10 (red), 1/25 (orange), 1/50 (green) and 1/100 (blue) of the maximum field.

machines would certainly be smaller and lighter. Different configurations, such as positioning all coils in one cryostat, in separate cryostats or a using combination of different superconducting wires are possible and might have some advantages in size and efficiency. The shielding coils are normally operating in a much lower field region than the main and cancelling coils, allowing higher critical current densities in the shielding coils. In some cases the use of a different type of wire for the shielding coils reduces costs and simplifies the cryostat. Our test motor machine does not have active shielding coils due to its operation in a laboratory environment and the comparably low working magnetic fields of the device.

4. Liquid metal sliding contact

Homopolar machines are characterised by intrinsically low voltages, high operating currents and substantial sliding contact surface speeds making current transfer between moving and stationary parts a challenging task. LMCC are a solution, as they are capable of transferring high currents (tens of thousands of Amperes) at very high surface speeds in the order of 100 m s^{-1} with virtually no mechanical wear and reasonably low friction. In the LMCC a conducting liquid is used to transport the current between the stationary and moving parts. The liquid has to have certain properties, including a low melting point, high boiling temperature, good conductivity, low density and low viscosity, for stable and efficient operation. Table 2 summarises the physical properties of three materials that are liquid at room temperature and that have been used in similar applications.

Toxicity, chemical reactivity and safety are additional important factors, beside the physical properties, for the best choice of material. Table 3 compares the main advantages and disadvantages of the different materials mentioned above. It can be seen that there is no ideal material and depending on the application different liquids can be preferable.

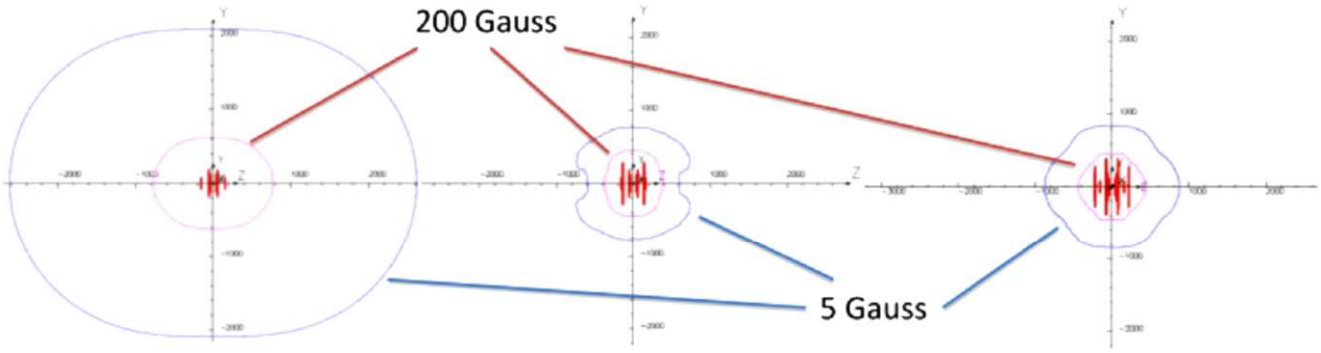

Figure 6. 200 and 5 Gauss boundary lines for an unshielded and a 2 and 4 shielding coil arrangement. All machines are designed to have the same performances and maximum magnetic field (6 T).

LMCCs can be divided into self-excited closed systems and systems were the liquid is pumped through an external loop. The advantages of looped systems include the ability to implement filtering and cooling stages as well as liquid metal reservoirs outside of the machine to continuously clean and cool the liquid leading to better performance and greater reliability. Self-excited closed systems have restricted cooling capabilities and hence they are not suitable for high power applications. Liquid metals are excellent cooling fluids due to their outstanding thermo-physical properties, especially sodium–potassium which is well known as a preferred cooling liquid in high performance applications. A similar approach was used by General Electric for their 60 MW generator that consisted of six identical 10 MW and 150 kA drum-type homopolar generators [11], each equipped with two independent sodium–potassium cooling loops allowing for partial heat removal from the motor. Another technological challenge is the deterioration of the liquid metal over extended periods of time due to gradual reaction with contaminants, especially during operation at elevated temperatures. Degradation of the liquid metal directly effects the performance of the LMCC and therefore liquid metal quality must be maintained for stable long term operation. This can be achieved by introduction of filters and spare liquid reservoirs into the recirculation loop. The SEGMAG prototype by Westinghouse Research Laboratories (3000 HP, 107 kA and 20 V) was also equipped by a NaK loop for recirculation and purification of the liquid, which allowed up to 9000 h continuous operation with various contamination levels of cover gas [12], [13].

A further differentiation can be made between spray and continuous LMCCs. The spray systems only have a beam of liquid focused on the rotor which allows very high current densities whilst continuous LMCCs have maximum current surface contact area due to the entrainment of the liquid metal around the circumference of the rotor/stator gap.

The test motor employed a self-excitation system (figure 7) that uses the frictional drag and centrifugal force that is applied to the liquid metal during operation of the machine to entrain the liquid metal between the rotor and stator contact surfaces. The rotor tip and stator form a thin channel that guides the liquid around the circumference at operational speeds. The sealed contacting area has to be filled with the liquid only once and the liquid collects at the bottom of the system during stoppages (figure 8). Due to friction the liquid will be distributed around the rotor and stator circumference when the rotor achieves a certain speed. This allows an evenly distributed current flow in the rotor disc and maximum contact area. In some cases the starting current has to be limited to avoid overloads and local heating due to the channel not being completely filled as the liquid has not yet been completely distributed around the channel. Magnetic fields in the contact area lead to additional forces acting on the liquid which can force the liquid out of the contact area or create additional drag. These additional forces result in unstable operation or high losses in the machine.

The contact area has to be designed to suit the operational parameters by varying the contact width, gap and surface material. A full discussion on the optimisation of the contact geometry and material would go beyond the scope of this manuscript. However, some of the basic relationships which have to be considered are:

- Frictional losses are proportional to the liquid density and the third power of the surface speed (figure 9).
- The loss distribution between mechanical and electrical losses is determined by the volume of liquid in the contact (more liquid means less electrical losses and more mechanical losses).
- The total LMCC resistance is mainly determined by the solid-liquid interface resistance (typically 2/3 of total resistance).
- At low currents the main losses arise from frictional effects and therefore the amount of liquid used should be minimised.

5. Test motor

We have designed, developed and built a 200 kW disc-type homopolar superconducting DC motor as a proof of concept and to demonstrate our technology (figure 10). The concept is based on a split-pair high-temperature superconducting magnet that can generate an average axial magnetic field of

Table 2. Relevant physical properties of NaK, Galinstan and Mercury for the operation in LMCC.

	NaK	Galinstan	Mercury
Material	Sodium–potassium 78 alloy	Gallium–indium–tin eutectic alloy	Mercury
Melting point (°C)	−12.6	−19	−38.8
Boiling point (°C)	785	>1300	356
Density (g cm^{-3})	0.866	6.44	13.53
Viscosity (Pa s)	0.546×10^{-3}	2.4×10^{-3}	1.55×10^{-3}
Resistivity at 20 °C (Ω m)	41×10^{-8}	29×10^{-8}	98×10^{-3}

Table 3. Choice of liquid metal.

	Advantages	Disadvantages
NaK	(1) High electrical conductivity	(1) Chemically active, reacts with water and oxygen. Inert atmosphere is required for stable contact operation
	(2) Low density and viscosity	
	(3) Liquid at room temperature	
	(4) High heat conductivity	
Galinstan	(1) Highest electrical conductivity	(1) High density, not suitable for high speed applications
	(2) Liquid at room temperature	(2) Incompatible with aluminium
	(3) Non-toxic	(3) very expensive
Mercury	(1) Lowest melting point	(1) Low boiling temperature
	(2) Good viscosity	(2) Toxic vapour
	(3) Chemical very stable	

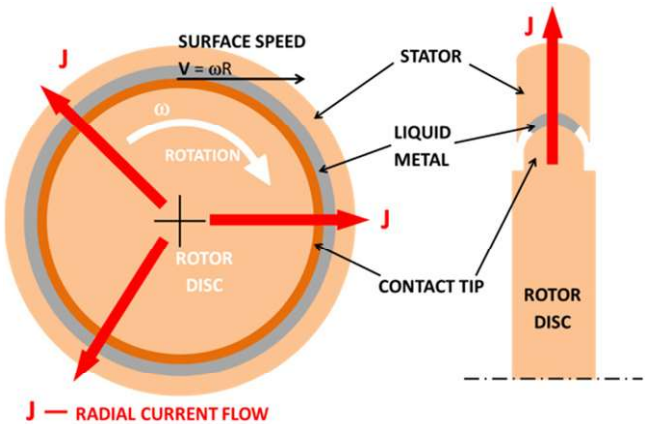

Figure 7. Sketch of a simple self-excitation liquid metal current collector system.

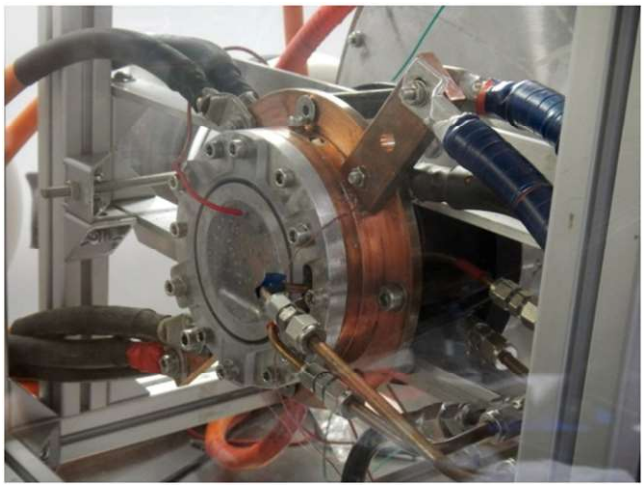

Figure 8. Picture of liquid metal current collector test assembly with a window on the side where the liquid metal can be seen collected on the bottom.

around 1 T and implements cancelling coils as well as a newly developed LMCC system. The motor design parameters are summarised in table 4.

5.1. Design

Each of the magnets consists of a mirror-inverted coil arrangement of one main coil and two cancelling coils (figure 4). The magnet was designed and built in cooperation with HTS-110 Ltd in New Zealand to allow different test configurations and experiments. Hence, the magnet size and weight are not optimised and allow room for future improvements and design changes to the rotor system. The overall dimensions of the magnet pair is 900 mm × 900 mm × 760 mm (width × height × length) and it has a warm bore diameter of 290 mm. Sumitomo DI-BSCCO wire was used to wind several pancake coils that

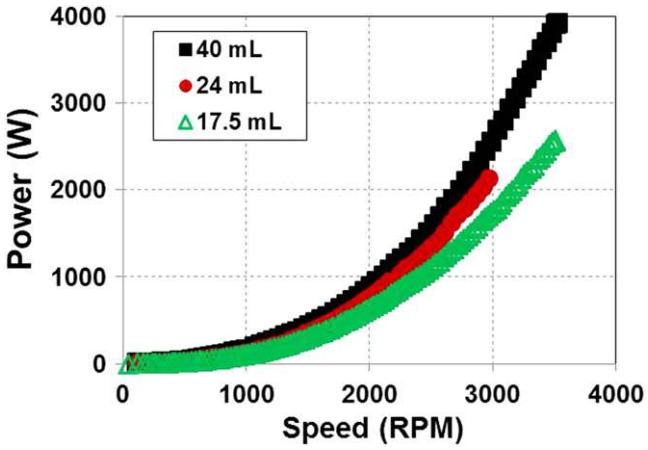

Figure 9. Friction losses measured on our test current collector for different amount of NaK liquid and rotational speeds.

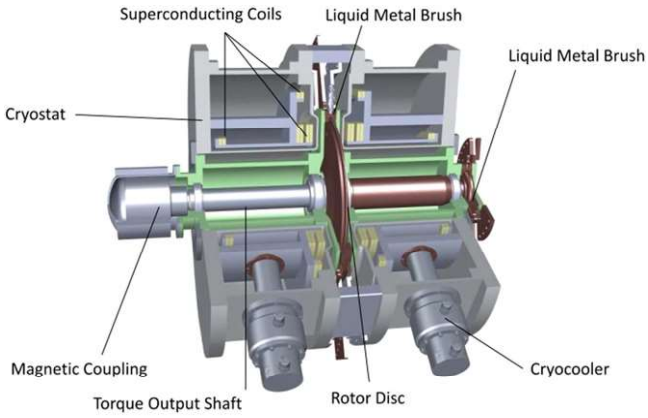

Figure 10. Test motor design drawings.

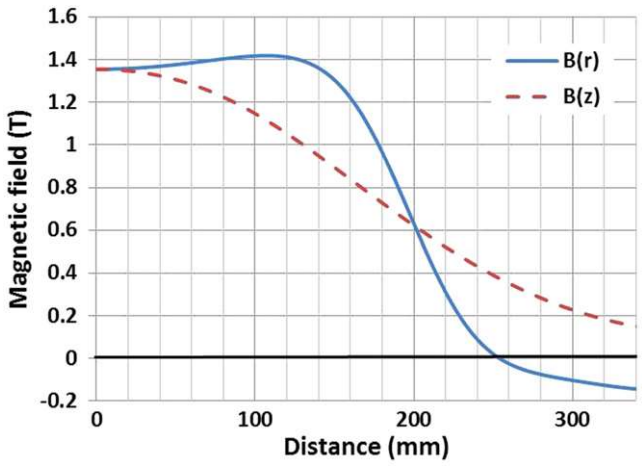

Figure 11. Magnetic field along centre of the magnet in radial direction (blue) and magnetic field along the axis (red).

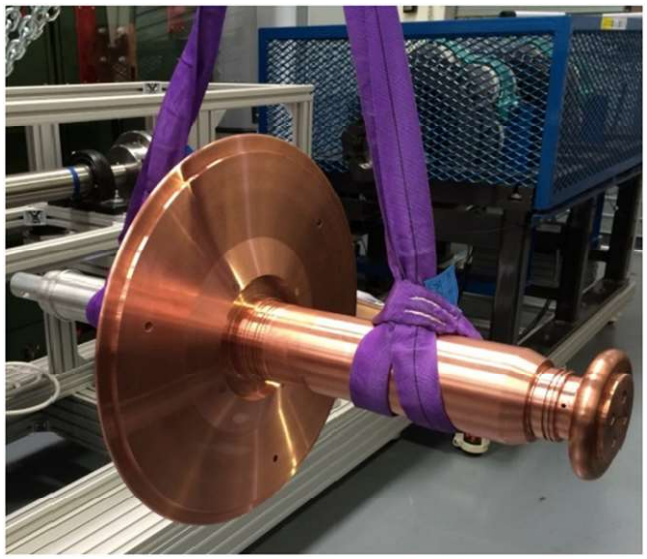

Figure 12. Copper rotor built out of a single billet.

Table 4. Maximum motor design parameters.

Power at rated speed (kW)	200
Maximum speed (RPM)	3600
Current (A)	20 000
Voltage (V)	10
Torque (Nm)	530
Weight (estimated) (kg)	700
Overall sizes (w × h × l) (m)	1.0 × 1.0 × 1.0

were connected in series. The wire specification allows a maximum magnet operating temperature of 30 K at design current (160 A) which corresponds with a maximum field of 2.4 T on the main coils. A solution with two separate cryostats and cryocoolers was chosen to allow maximum flexibility during operation and testing. The magnetic field along the radius ($B(r)$) in the centre between the two magnets, which is important for the voltage and torque calculations of the machine, has a maximum of 1.3 T at 110 mm (figure 11) and reaches a zero field crossover at 250 mm where the LMCC are situated. The full field profile can be seen in figure 4.

The copper rotor disc was built out of a single billet and designed to carry the maximum design current and mechanical load (figure 12). The outer diameter of the disc is 500 mm and the shaft diameter is 100 mm. In figure 12 the different shape and size of the outer and inner sliding contact tips can be seen. Each of these is optimised for the different current densities due to their different circumferences. The rotor is fully enclosed within an air-tight composite envelope and a magnetic coupling is used to transmit the output torque outside of this envelope. This enclosure is used to contain the inert cover gas atmosphere needed to prevent oxidisation of the liquid metal in a very reliable way as there are no sliding seals. Since sodium–potassium alloy is reactive with moisture and oxygen, the rotor envelope has to be air-tight and filled with slightly over-pressurised high-purity argon gas. Nitrogen gas can also be used for this purpose.

We developed a sodium–potassium liquid metal current collector allowing stable electric contact between the rotor and stator at surface speed up to 100 m s^{-1} and current densities of 250 A cm^{-2}. The stator is actively cooled by fluid that flows through pipes incorporated into the copper stator. The rotor is only cooled by the LMCC and heat transfer

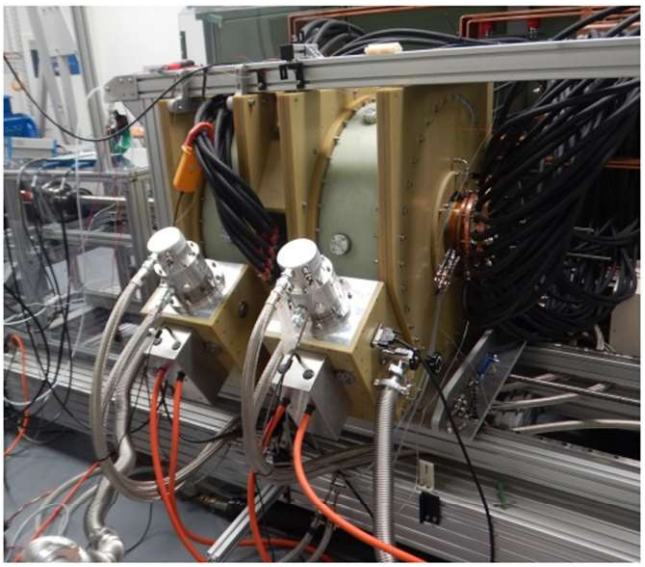

Figure 13. Full motor assembly with the two magnet halves, rotor housing and power cable.

through the argon gas. The fully assembled motor can be seen in figure 13.

Estimates of the mechanical and electrical losses generated by the LMCC were made and they are shown together with the power requirements for the cryogenic and water circulation cooling system in table 5. The LMCC losses were calculated from equations that combine the resistive and hydrodynamic losses in a solid-liquid-solid transition. Similar calculations were performed for our test assembly (figure 8) and they compared favourably with our measured results. A total power of 30 kW was calculated for the system to supply cooling and overcome loss during operation. This results in an efficiency of above 85% for a system that is not fully optimised. Some of the power required for the cryogenic system is not directly related to the working magnetic field strength of the device, an optimised 5 K low temperature magnet system requires similar cooling power but can double the working magnetic field strength. The magnetic field can be also increased by replacing the superconducting wire with coated conductors which have higher critical fields. Increasing the working magnetic field is a good way of improving the overall efficiency of the motor.

5.2. First test results

The motor was tested under different load conditions using a 300 kW air-cooled eddy current dynamometer and a 240 kW DC power supply that can deliver up to 20 000 A at 12 V. To date only preliminary tests have been performed on the motor and more testing is scheduled for the next year. The motor design specifications were achieved during short-term testing and the fundamental theoretical relationships and our design calculations were confirmed. Figure 14 shows the torque curves for different motor operating currents and for different operating currents of the superconducting excitation magnet (magnetic field levels). A maximum torque of 532 ± 5 Nm could be achieved at the rated maximum motor current of

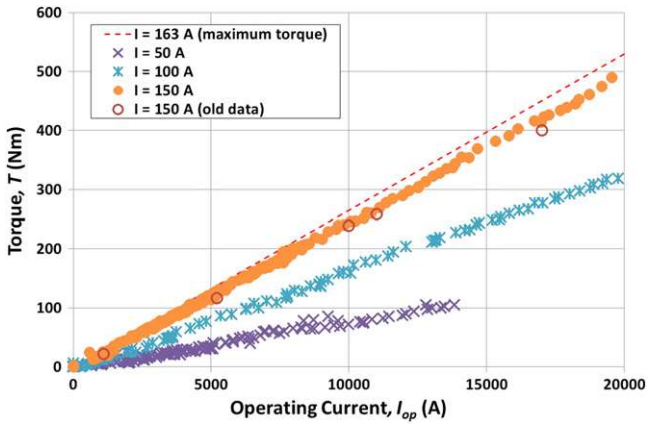

Figure 14. Torque versus rotor operating current for different excitation magnetic fields (I_{SC} magnet operating current). The symbols indicating measurement points and the lines are linear interpolation of the measurements.

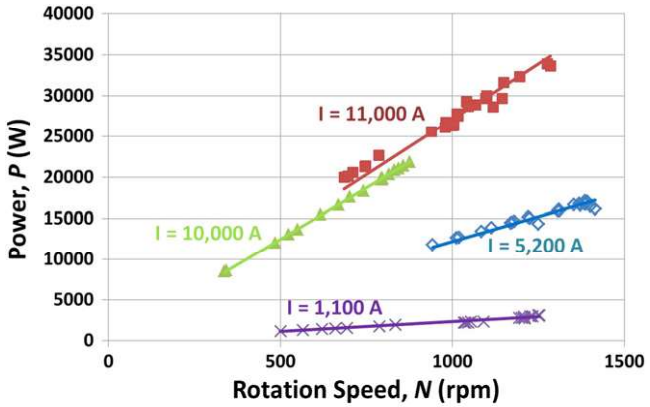

Figure 15. Power versus speed for different operating currents. The symbols indicating measurement points and the lines are linear interpolation of the measurements.

Table 5. Losses estimations by source.

Mechanical losses (kW)	5
Electrical losses (kW)	2.5
Water cooling system (kW)	1.5
Cryogenic cooling (kW)	14
Compressor cooling (kW)	6
Vacuum Pump (kW)	1
Total (kW)	30
Efficiency (%)	~86

20 000 Amps. The figure shows good linear dependence between current and torque, as well as the magnetic field.

The power and speed relationship is also linear as shown for two different operating currents in figure 15. A maximum rotation speed of around 3100 rpm was achieved during preliminary tests. However we had to limit further testing to a maximum speed of 1500 rpm due to limitations of our current test equipment and facilities.

Figure 16 shows the speed, current and power of a motor test over more than 1.5 h. The motor was operated at a constant current and load to measure the stability of operation.

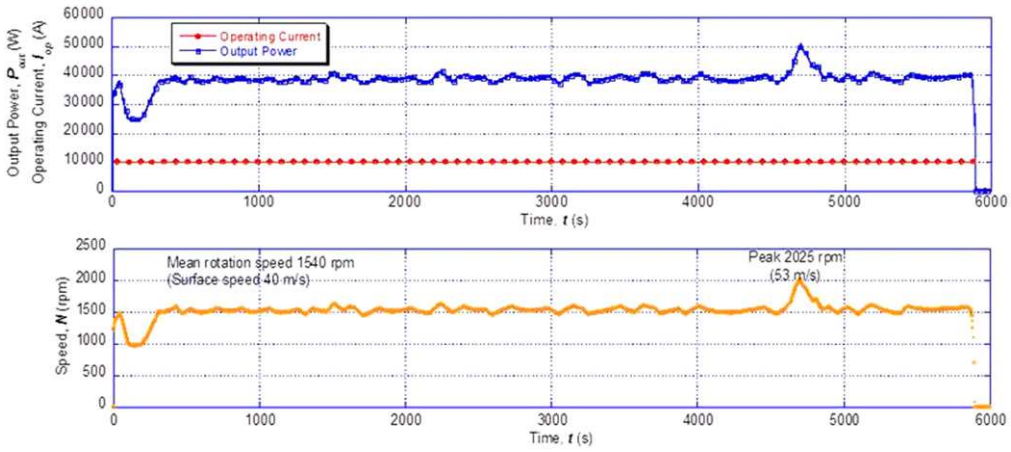

Figure 16. Continuous testing with high operating current and constant power output: $I_{op} = 10$ kA, $I_{sc} = 150$ A, $P = 38.5$ kW, $N = 1540$ rpm.

However, the test dynamometer had no feedback loop which could adjust for variations in the operating current or changes in the load due to a temperature increase in the dynamometer. Hence, the power output varied over the time slightly and some peaks were measured. At the beginning of the test it is very difficult to set the load values correctly and manual adjustments to the dynamometer have to be made resulting in some inhomogeneity. The large peak appearing around 4700 s was the result of a short speed runaway due to overheating of the dynamometer. Average electro-mechanical conversion efficiency (excluding cryogenic and water cooling) of 93% was achieved during this test.

Longer term stable operation at higher operating currents of 15–20 kA was also demonstrated. The longest operation time was over two hours at an operating current of 16 kA occurred during counter-EMF measurements at various speeds and magnetic field levels (1, ½, ¼ and $\frac{1}{8}$ of the full field). The data from this testing is shown in figure 17. As with the torque testing, excellent linear dependence was achieved with high degree of confidence. Interception with vertical axis of all three curves is determined by the Ohmic voltage component, allowing estimation of the stator-to-stator internal resistance of about 9.4 $\mu\Omega$. The voltage expected at 60 revolutions per second (3600 rpm) at full field is 10.3 V.

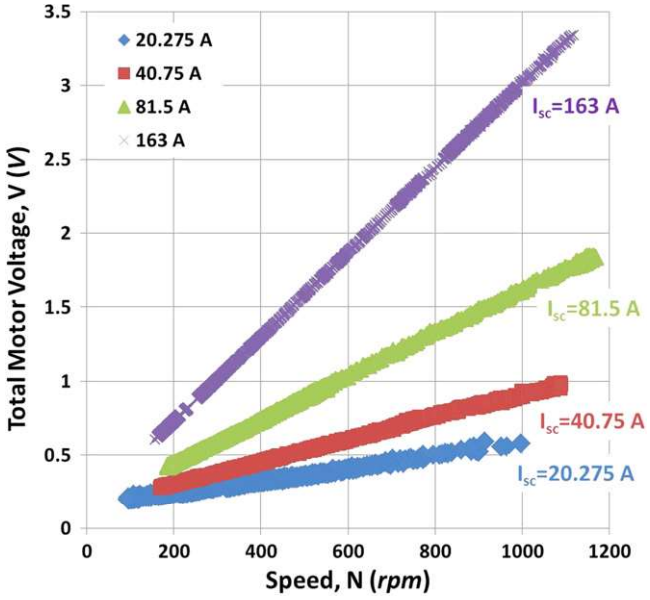

Figure 17. Stator-to-stator voltage of the motor: $I_{op} = 16$ kA, $P = 0.5 \div 61$ kW, $N = 100 \div 1100$ rpm, $I_{sc} = 163$, 81.5, 40.75 and 20.375 A (1, ½, ¼, and $\frac{1}{8}$ of the maximum current of HTS excitation coils).

6. Conclusion

We have developed and tested a new superconducting homopolar motor and generator which has a specially designed magnetic field profile. This field profile is produced by a unique arrangement of coils that creates a high drive field for the rotor and a low field regions for the field critical LMCC. The use of DC magnetic fields allows the utilisation of well-known magnet technology to build efficient cryogenic systems. Multi-physics software was used to optimise the coil design and analyse the motor's performance. The LMCC was specially designed to fit in the low field regions and allow very high current densities and surface speeds.

We have built a 200 kW test motor to demonstrate our technology and serve as a future test platform. The motor was tested under different conditions confirming all of the main design parameters. Further testing is scheduled to get a full understanding of the motor's behaviour under different dynamic load conditions and during long term operation.

The approach presented in this manuscript was used to produce design concepts for different homopolar motors and generators for selected applications. Motor applications that require high torque and low speeds or generator applications involving large currents seem to be highly suitable for this type of machine. Homopolar motors for electric ship propulsion or trains are possible and might have the added advantage of using direct integrated DC power sources (fuel

cell, batteries). Wind Turbine generators using homopolar generator technology could be directly connected to the DC grids currently used underwater or long distance cables. The combination of superconducting cables, liquid hydrogen energy storage and DC homopolar generators can allow a very efficient energy grid. Finally, DC homopolar generators could be used where an efficient high current source is required such as in smelting applications.

References

[1] Watt D A 1956 A homopolar generator for high current low voltage d supply *Atomic Energy Research Establishment Report* ED/R 1843 Declassified edition of AERE CE/R 821, 1951 (52)

[2] Crawford T J 1950 Homopolar generator for resistance welding *Weld. J.* **29** 211

[3] Lamme B G 1912 Development of a successful dc. 2000 kW unipolar generator *Trans. Am. I.E.E.* **31** 1811

[4] Ugrimoff B 1910 *Die unipolare Gleichstrommachine* (Berlin: Springer)

[5] Klaudy P 1961 Fortschritte im bau von unipolarmaschinen durch anvendung fon flussigkeitskontacten *Electrotech. Mach.* **78** 123–43

[6] Kuhlmann-Wilsdorf D 1999 Metal fiber brushes *Electrical Contacts* ed P G Slade (New York: Marcel Dekker) p 943

[7] Headifen G R, Pappas J A, Weldon J M, Wright J C, Price J H and Gully J H 1993 Preliminary design of a 1 GJ homopolar generator *IEEE Trans. Magn.* **29** 980–5

[8] Gubser D 1996 Superconducting homopolar motor and conductor development *J. Miner. Met. Mat. Soc.* **48** 30–4

[9] Thome R J, Creedon W, Reed M, Bowles E and Schaubel K 2002 Homopolar Motor Technology Development *Power Engineering Society Summer Meeting* vol 1 pp 260–4

[10] Guina A, Kells J, Labes K, Sercombe D, Lissington T, Fuger R, Matsekh A and Geronimo C Electromagnetic Turbine *Australian Patent* 2015201800 (Filed 2015)

[11] 1962 150 000 continuous D C amperes easy for acyclic generator *Power Eng.* **66** 1

[12] Witkowski R E, Arcella F G and Keeton A R 1976 Vital support systems for liquid metal collector homopolar machines *IEEE Trans. Power Appar. Syst.* **PAS-95** 1493–500

[13] Johnson J L, Humbert G T and Keeton A R 1976 Liquid metal current collectors for homopolar machines *IEEE Trans. Power Appar. Syst.* **PAS-95** 1234–43